

On Extracting Thermal Parameters and Scenario in High-Energy Collisions

Ting-Ting Duan^{1,a)}, Sahanaa Büriechin^{1,b)}, Hai-Ling Lao^{2,c)}, Fu-Hu Liu^{1,d)}, Khusniddin K. Olimov^{3,4,e)}

¹*State Key Laboratory of Quantum Optics and Quantum Optics Devices, Institute of Theoretical Physics, Shanxi University, Taiyuan 030006, China*

²*Department of Science Teaching, Beijing Vocational College of Agriculture, Beijing 102442, China*

³*Laboratory of High Energy Physics, Physical-Technical Institute of Uzbekistan Academy of Sciences, Chingiz Aytmatov Str. 2b, Tashkent 100084, Uzbekistan*

⁴*Department of Natural Sciences, National University of Science and Technology MISIS (NUST MISIS), Almalyk Branch, Almalyk 110105, Uzbekistan*

Abstract: In this minireview article, we examine the inconsistent results of thermal parameters derived from various models in high-energy collisions. Through a comprehensive literature review and based on the average transverse momentum $\langle p_T \rangle$ or the root-mean-square transverse momentum $\sqrt{\langle p_T^2 \rangle}$, we propose model-independent parameters to address these inconsistencies. The relevant parameters include: the initial temperature $T_i \approx \sqrt{\langle p_T^2 \rangle}/2$, the effective temperature $T = \langle p_T \rangle$, the kinetic freeze-out temperature $T_0 = \langle p_T \rangle/3.07$, and the average transverse velocity $\beta_T = (2.07/3.07)\langle p_T \rangle/\langle m \rangle$, where $\langle m \rangle$ represents the average mass of moving particles in the rest frame of the emission source. Our findings indicate that these four parameters are larger in central collisions, within central rapidity regions, at higher energies, and in larger collision systems. As collision energy increases, excitation functions for all four parameters rise rapidly (slowly) within ranges below (above) approximately 7.7 GeV. At higher energies (> 39) GeV, fluctuations occur in trends for these excitation functions, with only slight changes observed in their growth rates. Additionally, this work reveals a mass-dependent multi-temperature scenario pertaining to both initial states and kinetic freeze-out processes.

Keywords: High-energy collisions; Average transverse momentum; Root-mean-square transverse momentum; Thermal parameters; Mass dependent multi-temperature (scenario)

PACS numbers: 12.40.Ee, 13.85.Ni, 13.87.Ce

a) 202312602001@email.sxu.edu.cn

b) 202201101236@email.sxu.edu.cn

c) hailinglao@163.com ; hailinglao@pku.edu.cn

d) Correspondence: fuhuliu@163.com ; fuhuliu@sxu.edu.cn

e) Correspondence: khkolimov@gmail.com ; kh.olimov@uzsci.net

1. Introduction

High-energy collisions represent a significant area of research in modern physics, wherein a hot and dense system can be generated. This system subsequently undergoes a hadronization process [1]. Currently, high-energy collisions are primarily conducted at the Brookhaven National Laboratory (BNL) in the USA, covering an energy range from several GeV to 200 GeV, and at the European Organization for Nuclear Research (CERN) in Switzerland, which operates within an energy range from several GeV to nearly 20 GeV and from several TeV to over 10 TeV [2-5]. Additionally, related collisions at lower energies are anticipated to become available soon at the Helmholtzzentrum für Schwerionenforschung GmbH (GSI) in Germany and the Joint Institute for Nuclear Research (JINR) in Russia [6, 7].

In the final state of high-energy collisions, numerous particles are produced; however, some particles emerge throughout the entire collision process, i.e., from initial state to final state. The final state also marks the stage of kinetic freeze-out during system evolution. When extracting thermal or related parameters such as kinetic freeze-out temperature (T_0) and average transverse flow velocity (β_T), various types of particles contribute differently based on their respective transverse momentum (p_T) regions.

It is commonly believed that the vast majority of particles are thermally produced in the final state via soft process and are distributed in the region of low- p_T [8-12]. In contrast, a very small number of particles are directly produced in the initial state via hard process and are distributed throughout the entire p_T region. The number of particles produced in the intermediate state falls in the middle, distributed in the region of low- and intermediate- p_T . Clearly, particles with low- p_T (high- p_T) make a significant (minor) contribution to the parameters, while particles with intermediate- p_T contribute moderately to the parameters.

Based on varying fit ranges for the same p_T spectrum, the parameters extracted from identical models or distributions may differ to some extent, not to mention the discrepancies arising from employing different spectra and models. In particular, utilizing a blast-wave model across diverse fit ranges in the low- p_T region [13, 18-20], combined with other models for the high- p_T region, has led to observations of particle production that may exhibit single, double, or multiple T_0 values [12-14]. This suggests potential scenarios involving single, double, or multiple kinetic freeze-out processes in high-energy collisions [15-17].

In fact, when extracting temperature parameters using the blast-wave model [13, 18-20], if each fit range of the p_T spectrum is confined to narrow and specific regions corresponding to different types of particles, one can derive a singular scenario. Conversely, if temperature parameters for strange and non-strange particle spectra are found to be distinct from one another, this could yield a dual scenario. Should each fit range of the p_T spectrum be maximized in width as much as possible, it may result in a multiple scenario that generally depends on particle mass. Furthermore, by employing alternative models such as the improved Tsallis distribution [16, 21] and intercept-slope methods [19, 22-25], inconsistent temperatures might also be

obtained. Thus, it follows that kinetic freeze-out scenarios are inherently dependent on both fit range and model selection.

Additionally, the question of whether T_0 is greater in central versus peripheral collisions; within central compared to forward/backward rapidity regions; at low versus high energies; as well as between small versus large collision systems remains contingent upon various modeling factors that influence these results [26, 27]. Moreover, the existence of either positive or negative correlations between T_0 and β_T is also an issue closely tied to specific modeling approaches.

In this work, we propose a method to extract the initial temperature (T_i), effective temperature (T), T_0 , and β_T based on the average transverse momentum $\langle p_T \rangle$ and root-mean-square transverse momentum $\sqrt{\langle p_T^2 \rangle}$ across the entire p_T range. This approach is informed by literature research and yields consistent results for different cases, supporting the existence of multiple temperature scenarios for particle formation and kinetic freeze-out [15, 16, 28, 29].

The remainder of this article is structured as follows: Section 2 introduces single- and multi-component distributions. In Section 3, we describe model-independent thermal parameters. A discussion on parameter trends is presented in Section 4. Finally, Section 5 provides a summary and conclusion.

2. Single- and multi-component distributions

Experimental distributions related to p_T typically take three forms: invariant yield, unit-density of rapidity (y) and p_T , as well as density of p_T . Let E denote energy, p represent momentum, m_T signify transverse mass for a given particle, and N indicate the number of particles; these three forms can be expressed as $E d^3N/d^3p = (1/2\pi p_T)(d^2N/dydp_T) = (1/2\pi m_T)(d^2N/dydm_T)$, $d^2N/dydp_T$, and dN/dp_T , respectively. If experimental data presents p_T -related distributions in alternative formats, one may convert these non-canonical representations into one of the aforementioned three forms.

In certain instances where experimental data exhibits narrow ranges in p_T values, a single-component function may suffice to describe or fit these distributions effectively. For example, in proton-proton, proton-nucleus, and nucleus-nucleus collisions conducted at center-of-mass energies per nucleon pair ($\sqrt{s_{NN}}$) ranging from several GeV to over 10 TeV, one can utilize single-component standard (Bose-Einstein or Fermi-Dirac) distribution to approximate experimental data within the region where $p_T < 2 - 3$ GeV/ c , in which the particles are produced in the soft excitation process.

The single-component standard distribution arises from the relativistic ideal gas model. The invariant yield is expressed as [30]

$$E \frac{d^3N}{d^3p} = \frac{gV}{(2\pi)^3} E \left[\exp\left(\frac{E - \mu}{T}\right) + S \right]^{-1}, \quad (1)$$

where g and μ represent the degeneracy factor and chemical potential of a given particle, respectively. Additionally, V and T denote the volume and effective temperature of the interaction system. Here, $S = -1$ corresponds to the Bose-Einstein distribution, while $S = 1$ pertains to the Fermi-Dirac distribution. The unit-density for y and p_T is formulated as

$$\frac{d^2N}{dydp_T} = \frac{gV}{(2\pi)^2} p_T \sqrt{p_T^2 + m_0^2} \cosh y \left[\exp\left(\frac{\sqrt{p_T^2 + m_0^2} \cosh y - \mu}{T}\right) + S \right]^{-1}, \quad (2)$$

with m_0 indicating the rest mass of the specified particle. In Eq. (1), E appears in Eq. (2) in terms of y and p_T via $E = m_T \cosh y$, where $m_T = \sqrt{p_T^2 + m_0^2}$ is defined as the transverse mass. The density for p_T is given by

$$\frac{dN}{dp_T} = \frac{gV}{(2\pi)^2} p_T \sqrt{p_T^2 + m_0^2} \int_{y_{\min}}^{y_{\max}} \cosh y \left[\exp\left(\frac{\sqrt{p_T^2 + m_0^2} \cosh y - \mu}{T}\right) + S \right]^{-1} dy, \quad (3)$$

wherein experimental rapidity bins $[y_{\min}, y_{\max}]$ serve as lower and upper limits for integration over y .

In Eqs. (1)-(3), T serves as the sole free parameter while V acts as a normalization constant. Although μ does not significantly influence fits related to distributions involving p_T , it can be derived through either particle ratios or traditional methods. The former approach relies on calculating ratio (K_j) between negatively charged particles to positively charged ones alongside source's corresponding temperature (T_j) at that moment: $\mu = -(1/2)T_j \ln K_j$ [12, 31-33]. The latter method utilizes three net quantum numbers (net-baryon number B , strangeness S , and electric charge Q) alongside their respective chemical potentials (μ_B , μ_S , and μ_Q): $\mu = B\mu_B + S\mu_S + Q\mu_Q$ [12, 34-40].

It is recognized that a single-component standard distribution may not adequately describe extensive distributions related to p_T observed in experiments; thus, consideration should be given to two- or multi-component standard distributions instead. For an n_0 -component standard distribution scenario, one can express invariant yield as

$$E \frac{d^3N}{d^3p} = \sum_{i=1}^{n_0} E \frac{d^3N_i}{d^3p} = \sum_{i=1}^{n_0} \frac{gV_i}{(2\pi)^3} E \left[\exp\left(\frac{E - \mu_i}{T_i}\right) + S \right]^{-1}, \quad (4)$$

where parameters such as N_i , V_i , μ_i , and T_i correspond to particle count, system volume, particle chemical potential, and source's effective temperature, respectively, associated with the i -th component. The unit-density for y and p_T takes form

$$\begin{aligned} \frac{d^2N}{dydp_T} &= \sum_{i=1}^{n_0} \frac{d^2N_i}{dydp_T} = \sum_{i=1}^{n_0} \frac{gV_i}{(2\pi)^2} p_T \sqrt{p_T^2 + m_0^2} \cosh y \\ &\quad \times \left[\exp\left(\frac{\sqrt{p_T^2 + m_0^2} \cosh y - \mu_i}{T_i}\right) + S \right]^{-1}. \end{aligned} \quad (5)$$

The density of p_T is given by

$$\begin{aligned} \frac{dN}{dp_T} &= \sum_{i=1}^{n_0} \frac{dN_i}{dp_T} = \sum_{i=1}^{n_0} \frac{gV_i}{(2\pi)^2} p_T \sqrt{p_T^2 + m_0^2} \int_{y_{\min}}^{y_{\max}} \cosh y \\ &\quad \times \left[\exp \left(\frac{\sqrt{p_T^2 + m_0^2} \cosh y - \mu_i}{T_i} \right) + S \right]^{-1} dy. \end{aligned} \quad (6)$$

In Eqs. (4)-(6), the free parameters are denoted as T_i . Generally, a value of $n_0 = 2$ or 3 is sufficient for fitting the data; thus, an excessively large n_0 is unnecessary.

In the preceding discussion, although n_0 components may exhibit similar forms of standard distribution with varying parameters due to the inherent similarities, commonalities, and universal characteristics observed in high-energy collisions [41-48], increasing the number of free parameters and normalization constants associated with larger values of n_0 ultimately reduces the degrees of freedom (ndof), which deviates from our expectations. Instead, one might consider employing the Tsallis distribution [30, 49-54] to encapsulate multi-component standard distributions.

Within the framework of the Tsallis distribution [30, 49-54], invariant yield, unit-density of y and p_T , as well as density of p_T are represented by

$$E \frac{d^3N}{d^3p} = \frac{gV}{(2\pi)^3} E \left\{ \left[1 + (q-1) \frac{E - \mu}{T} \right]^{\frac{1}{q-1}} + S \right\}^{-q}, \quad (7)$$

$$\begin{aligned} \frac{d^2N}{dy dp_T} &= \frac{gV}{(2\pi)^2} p_T \sqrt{p_T^2 + m_0^2} \cosh y \\ &\quad \times \left\{ \left[1 + (q-1) \frac{\sqrt{p_T^2 + m_0^2} \cosh y - \mu}{T} \right]^{\frac{1}{q-1}} + S \right\}^{-q}, \end{aligned} \quad (8)$$

and

$$\begin{aligned} \frac{dN}{dp_T} &= \frac{gV}{(2\pi)^2} p_T \sqrt{p_T^2 + m_0^2} \int_{y_{\min}}^{y_{\max}} \cosh y \\ &\quad \times \left\{ \left[1 + (q-1) \frac{\sqrt{p_T^2 + m_0^2} \cosh y - \mu}{T} \right]^{\frac{1}{q-1}} + S \right\}^{-q} dy, \end{aligned} \quad (9)$$

respectively. Herein, q denotes the entropy index that characterizes the degree of non-equilibrium within the interaction system. Typically, it holds that $q \geq 1$. The special case where $q = 1$ corresponds to equilibrium conditions under which the Tsallis distribution simplifies into its standard one. When q is much greater than 1, it indicates a high degree of non-equilibrium within the system. In practical analyses, it is often found that $q < 1.25$, suggesting that this value does not represent extreme non-equilibrium but rather indicates

approximate equilibrium conditions. In Eqs. (7)-(9), there exist two free parameters, T and q .

In certain instances where experimental distributions related to p_T span a wide range, a single or two-component Tsallis distribution may prove insufficient for adequately representing all data points. Consequently, consideration must be given to utilizing a multi-component Tsallis distribution which characterized by fewer components than would be required in a corresponding multi-component standard distribution when fitting identical datasets. The structure of this multi-component Tsallis distribution bears similarity to Eqs. (4)-(6); therefore, we will refrain from reiterating those details here.

Empirically speaking, fitting by the multi-component standard or Tsallis distribution can be achieved using a q-dual distribution [55]. With this context, invariant yield, unit-density of y and p_T , and density of p_T are denoted by

$$E \frac{d^3N}{d^3p} = \frac{gV}{(2\pi)^3} E \sum_{k=0}^{\infty} (-S)^k \left[1 + (k+1)(q-1) \frac{E-\mu}{T} \right]^{-\frac{q}{q-1}}, \quad (10)$$

$$\begin{aligned} \frac{d^2N}{dy dp_T} &= \frac{gV}{(2\pi)^2} p_T \sqrt{p_T^2 + m_0^2} \cosh y \sum_{k=0}^{\infty} (-S)^k \\ &\times \left[1 + (k+1)(q-1) \frac{\sqrt{p_T^2 + m_0^2} \cosh y - \mu}{T} \right]^{-\frac{q}{q-1}}, \end{aligned} \quad (11)$$

and

$$\begin{aligned} \frac{dN}{dp_T} &= \frac{gV}{(2\pi)^2} p_T \sqrt{p_T^2 + m_0^2} \int_{y_{\min}}^{y_{\max}} \cosh y \sum_{k=0}^{\infty} (-S)^k \\ &\times \left[1 + (k+1)(q-1) \frac{\sqrt{p_T^2 + m_0^2} \cosh y - \mu}{T} \right]^{-\frac{q}{q-1}} dy, \end{aligned} \quad (12)$$

respectively. In real analysis, a very large value of k is not necessary. In fact, setting the maximum k to 10 is sufficient for obtaining accurate results.

Naturally, one might consider that the multi-component q-dual distribution is well-suited for fitting the p_T -related distributions across an extensive range. The multi-component q-dual distribution shares similar summed forms with Eqs. (4)-(6), which will not be reiterated here. Nevertheless, transitioning from standard distribution to q-dual distribution allows for appropriate single-, two-, or multi-component models to fit the p_T -related distributions according to varying width ranges.

The multiple components represent various sources characterized by different excitation degrees or interaction mechanisms. Due to temperature variations among these sources, it becomes possible to measure temperature fluctuations ranging from the lowest temperature source (T_1), represented by the first component, up to the highest temperature source (T_{n_0}), described by the last (the n_0 -th) component. The average temperature of these n_0 sources can

be expressed as

$$T = \sum_{i=1}^{n_0} k_i T_i. \quad (13)$$

Here $k_i = N_i/N = V_i/V$ denotes the contribution ratio or fraction of the i -th component relative to all n_0 components and adheres to normalization such that $\sum_{i=1}^{n_0} k_i = 1$.

To illustrate the fitting effectiveness of the three types of distributions discussed above, as an example, Figures 1(a) and 1(b) present invariant yields of π^+ and π^- produced in $|y| < 0.1$ in gold-gold (Au+Au) collisions at $\sqrt{s_{NN}} = 200$ GeV. Different symbols represent experimental data measured by the STAR Collaboration [2] across various centrality intervals and scaled by distinct quantities indicated in each panel. The solid, dashed, and dotted curves correspond to results fitted using standard, Tsallis, and q-dual distributions with $S = -1$, respectively [12]. It is evident that all three distributions effectively describe the experimental data.

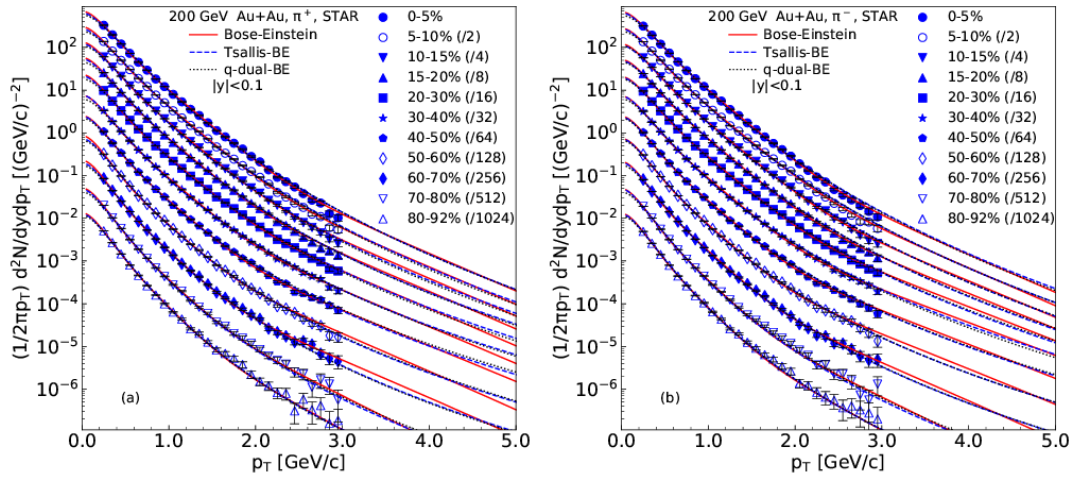


Figure 1. The invariant yields of (a) π^+ and (b) π^- produced in Au+Au collisions at $\sqrt{s_{NN}} = 200$ GeV. The symbols represent experimental data measured by the STAR Collaboration [2]. The solid, dashed, and dotted curves correspond to results fitted using standard, Tsallis, and q-dual distributions with $S = -1$, respectively [12].

The effective temperatures T presented in Figure 1 are illustrated in Figure 2 to examine the dependence of T on centrality percentage C . Panels (a) and (b) correspond to the results from the spectra of π^+ and π^- , respectively. Different symbols represent distinct values of T obtained from various distributions indicated in the panels. It is evident that all three values of T exhibit larger magnitudes in central collisions compared to peripheral collisions. However, these three temperatures show inconsistencies both in absolute values and trends, despite their ability to adequately describe experimental data. The discrepancies arise due to the influence

of another parameter, namely the entropy index q , within the Tsallis and q-dual distributions.

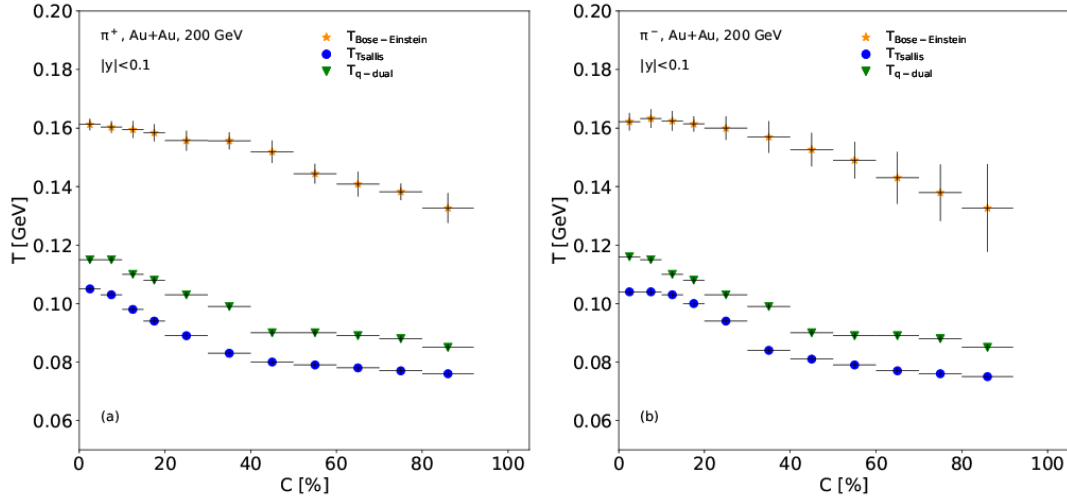


Figure 2. Dependence of T on C , where T is derived from standard, Tsallis, and q-dual distributions with $S = -1$, respectively. Panels (a) and (b) present results from π^+ and π^- spectra respectively.

It is important to note that the three distributions discussed above serve merely as examples for fitting experimental data. Other distributions, such as those derived from the blast-wave model [13, 18-20] and improved Tsallis statistics [16, 21], can also be employed for fitting purposes; however, it is possible that extracted temperatures may yield inconsistent results. Additionally, one might consider the p_T -exponential: $dN/p_T dp_T \propto \exp(-p_T/T)$, the p_T^2 -exponential or p_T -Gaussian: $dN/p_T dp_T \propto \exp(-p_T^2/T^2)$, the p_T^3 -exponential: $dN/p_T dp_T \propto \exp(-p_T^3/T^3)$, the m_T -exponential: $dN/m_T dm_T \propto \exp(-m_T/T)$, the Boltzmann: $dN/m_T dm_T \propto m_T \exp(-m_T/T)$, etc. [19], or their superpositions. Here, the effective temperatures T used in these expressions are different.

We would like to emphasize that while a variety of distributions can be utilized for fitting spectra related to p_T , the most fundamental remains the standard distribution derived from relativistic ideal gas model [30]. Nevertheless, in complex systems such as high-energy collisions, it is unrealistic to expect a single-component standard distribution will suffice. Instead, one should contemplate a multi-component standard distribution capable of accommodating multiple sources with varying degrees of excitation or interaction mechanisms. In real fitting, a standard distribution of two or three components is sufficient.

3. Model-independent thermal parameters

In our discussions above, it has been noted that T is dependent on model or distribution choice; this dependency can lead to different absolute values being reported. In particular, since T describes the degree of excitation within an interacting system at kinetic freeze-out, it

exhibits greater sensitivity towards model or distribution selection. Furthermore, many existing models or distributions have yet to disentangle contributions arising from thermal motion versus flow effect. Typically, the intensity of thermal motion is characterized by T_0 , while the magnitude of flow effect is represented by β_T .

The model-dependent parameters T_0 and β_T can lead to significantly inconsistent results. For instance, which value of T_0 is greater in central versus peripheral collisions? How does it compare between central and forward/backward rapidity regions? What about low-energy (e.g., 10 GeV) versus high-energy (e.g., 200 GeV) collisions? Additionally, how do small collision systems (e.g., proton-proton or proton-nucleus interactions) stack up against large ones (e.g., nucleus-nucleus collisions)? Are T_0 and β_T directly or inversely proportional? The answers to these questions often yield contradictions based on different models, such as the blast-wave model [13, 18-20] and thermal-related models [56, 57].

Generally speaking, the blast-wave model suggests a smaller value for T_0 in central collisions, at high energies, or within larger systems. In contrast, thermal-related models tend to present opposing conclusions. This discrepancy primarily arises from differing assumptions regarding flow profiles and varying fit ranges for p_T distributions [58]. The blast-wave model posits a flow that gradually increases from the inner core to the outer surface with particle-dependent fit ranges for p_T . Conversely, thermal-related models assume an invariant flow with broader fit ranges applicable across different particles.

To reconcile these contradictions or inconsistencies, one might consider employing average transverse momentum ($\langle p_T \rangle$) or root-mean-square transverse momentum ($\sqrt{\langle p_T^2 \rangle}$) as representations of thermal parameters. For any given set of data related to p_T , both $\langle p_T \rangle$ and $\sqrt{\langle p_T^2 \rangle}$ are independent of specific models or distributions; they can even be derived directly from empirical data. Before delving into the relationship between thermal parameters and either measure $\langle p_T \rangle$ or $\sqrt{\langle p_T^2 \rangle}$, we will first outline their respective representations based on the three distributions related to p_T mentioned above, as shown below.

Whether it is a single component or multiple components, from the distribution that can fit the relevant data of p_T , one can conveniently obtain $\langle p_T \rangle$ as

$$\langle p_T \rangle = \int_0^{p_{T\max}} \int_{y_{\min}}^{y_{\max}} p_T^2 E \frac{d^3 N}{d^3 p} dy dp_T / \int_0^{p_{T\max}} \int_{y_{\min}}^{y_{\max}} p_T E \frac{d^3 N}{d^3 p} dy dp_T, \quad (14)$$

$$\langle p_T \rangle = \int_0^{p_{T\max}} \int_{y_{\min}}^{y_{\max}} p_T \frac{d^2 N}{dy dp_T} dy dp_T / \int_0^{p_{T\max}} \int_{y_{\min}}^{y_{\max}} \frac{d^2 N}{dy dp_T} dy dp_T, \quad (15)$$

and

$$\langle p_T \rangle = \int_0^{p_{T\max}} p_T \frac{dN}{dp_T} dp_T / \int_0^{p_{T\max}} \frac{dN}{dp_T} dp_T \quad (16)$$

if the invariant yield, unit-density of y and p_T , and density of p_T are used, respectively. In particular, if the probability density function, $f(p_T) = (1/N)(dN/dp_T)$, is used, one has

$$\langle p_T \rangle = \int_0^{p_{T\max}} p_T f(p_T) dp_T / \int_0^{p_{T\max}} f(p_T) dp_T = \int_0^{p_{T\max}} p_T f(p_T) dp_T \quad (17)$$

due to the denominator in Eq. (17) being 1.

Go a step further, one has $\sqrt{\langle p_T^2 \rangle}$ in different forms,

$$\sqrt{\langle p_T^2 \rangle} = \sqrt{\int_0^{p_{T\max}} \int_{y_{\min}}^{y_{\max}} p_T^3 E \frac{d^3 N}{d^3 p} dy dp_T / \int_0^{p_{T\max}} \int_{y_{\min}}^{y_{\max}} p_T E \frac{d^3 N}{d^3 p} dy dp_T}, \quad (18)$$

$$\sqrt{\langle p_T^2 \rangle} = \sqrt{\int_0^{p_{T\max}} \int_{y_{\min}}^{y_{\max}} p_T^2 \frac{d^2 N}{dy dp_T} dy dp_T / \int_0^{p_{T\max}} \int_{y_{\min}}^{y_{\max}} \frac{d^2 N}{dy dp_T} dy dp_T}, \quad (19)$$

$$\sqrt{\langle p_T^2 \rangle} = \sqrt{\int_0^{p_{T\max}} p_T^2 \frac{dN}{dp_T} dp_T / \int_0^{p_{T\max}} \frac{dN}{dp_T} dp_T}, \quad (20)$$

and

$$\sqrt{\langle p_T^2 \rangle} = \sqrt{\int_0^{p_{T\max}} p_T^2 f(p_T) dp_T / \int_0^{p_{T\max}} f(p_T) dp_T} = \int_0^{p_{T\max}} p_T^2 f(p_T) dp_T. \quad (21)$$

If T can be directly obtained from $\langle p_T \rangle$, it is possible to derive a model-independent T . If T is proportional to $\langle p_T \rangle$ with a proportionality coefficient of 1, then we have $T = \langle p_T \rangle$. This definition is indeed model-independent.

Regarding T_0 , a straightforward approach is to assume that $T_0 = \langle p_T \rangle / \kappa$, where κ is a constant yet to be determined. In thermal-related models, one finds that $\kappa = 3.07$ [56, 57]. The remaining contribution to $\langle p_T \rangle$ should arise from flow effect. It follows that $\beta_T = (2.07/3.07) \langle p_T \rangle / \langle m \rangle$, where $\langle m \rangle = m_0 \langle \gamma \rangle$ is the average mass (energy), and $\langle \gamma \rangle$ is the average Lorentz factor of moving particles in the rest frame of the emission source. It is noted that $T_0 / \beta_T = m_0 \langle \gamma \rangle / 2.07$. Previous studies indicate that $\langle \gamma \rangle$ is less than 0.5% of the Lorentz factor for beam ions producing light flavor particles in TeV energy collisions [28]. Since both parameters, T_0 and β_T , discussed here are solely dependent on $\langle p_T \rangle$ derived from data, they are considered model-independent.

To our knowledge, there has been no discussion in existing literature regarding the relationship between T (T_0) and $\sqrt{\langle p_T^2 \rangle}$. Instead, research has focused on examining the connection between initial temperature T_i and $\sqrt{\langle p_T^2 \rangle}$ through color string percolation model [59-61]. According to this model, $T_i = \sqrt{\langle p_T^2 \rangle / 2F(\xi)}$, where $F(\xi) \approx 0.6 - 1$ represents the color suppression factor; a value of 0.6 corresponds to multiple strings with low probability while a value of 1 pertains to single string with high probability.

When considering only single string formed by two partons present within projectile and target ions respectively, we find $T_i \approx \sqrt{\langle p_T^2 \rangle} / 2$, which results in an approximate maximum reduction of 30% compared with $T_i = \sqrt{\langle p_T^2 \rangle / 2F(\xi)}$. In particle formation scenarios, it is most likely for two partons to predominantly participate in collisions, which may form single string. As an estimation, it can be accepted that $T_i \approx \sqrt{\langle p_T^2 \rangle} / 2$. Although this result arises from color

string percolation model [59-61], it remains solely data-dependent; thus, indicating that the use of T_i here maintains its model independence.

For unification purposes in this work, $\langle p_T \rangle$ and $\sqrt{\langle p_T^2 \rangle}$ are expressed in units of GeV/c . Other quantities are measured as follows: T_i , T , and T_0 are in GeV , while β_T is in c (with $c = 1$ within natural units).

Building upon this framework allows for the extraction of model-independent parameters. As an illustration, Figure 3 depicts the dependence of newly defined T on C as derived from Figure 1. Panels (a) and (b) present results corresponding to π^+ and π^- spectra respectively. Distinct symbols represent various values of T , each obtained from different distributions indicated within the panels. It is evident that all three values of T exhibit larger magnitudes in central collisions compared to peripheral collisions, a result consistent with observations related to $\langle p_T \rangle$. The three values demonstrate not only agreement in absolute terms but also similar trends across conditions within uncertain range; analogous behavior can be observed for T_i , T_0 , and β_T , details which will not be elaborated here due to their similarity.

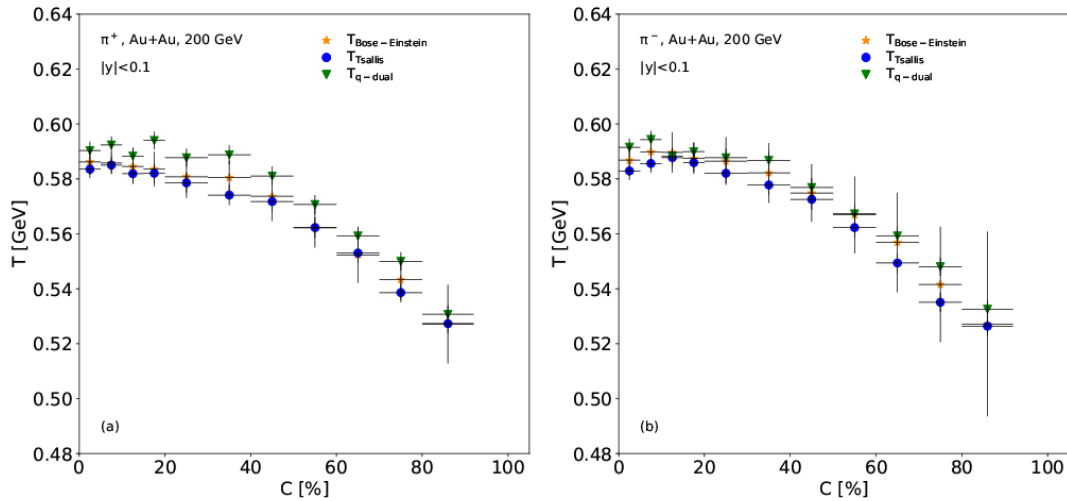


Figure 3. Dependence of T on C , where $T = \langle p_T \rangle$; this is based on standard, Tsallis, and q-dual distributions with $S = -1$, respectively. Panels (a) and (b) illustrate results from π^+ and π^- spectra respectively.

4. Discussion on parameter trends

We advocate for utilizing these model-independent parameters: T_i , T , T_0 , and β_T . These parameters have been extracted from either $\langle p_T \rangle$ or $\sqrt{\langle p_T^2 \rangle}$. Analyzing trends reported in literature regarding $\langle p_T \rangle$ and $\sqrt{\langle p_T^2 \rangle}$ reveals that both measures tend to be larger in central collisions than peripheral ones; they also increase with collision energy and system size when comparing large systems against small ones under various energy conditions respectively. This observation indicates that all four proposed parameters likewise manifest greater values under circumstances involving central collisions, higher energies, or larger systems, even though

some differences may appear minimal [26, 27, 62-65].

As for the rapidity dependence of $\langle p_T \rangle$ and $\sqrt{\langle p_T^2 \rangle}$, if the kinetic energy associated with longitudinal motion is accurately subtracted from the total energy of a given particle, it can yield reasonable results indicating that higher values of $\langle p_T \rangle$ and $\sqrt{\langle p_T^2 \rangle}$ are observed in the central rapidity region compared to the forward/backward rapidity regions. This observation suggests larger values of T_i , T , T_0 , and β_T in the central rapidity region due to a greater deposition of collision energies.

Utilizing model-independent parameters allows for consistent results across various collisions at different energies. The four parameter values are absolute rather than merely relative because they maintain model independence. Furthermore, since $\langle p_T \rangle$ and $\sqrt{\langle p_T^2 \rangle}$ depend on particle mass, these four parameters exhibit mass dependence. Consequently, this leads to multiple temperature scenarios; specifically, the mass-dependent T_i reflects multiple scenarios of initial state, while the mass-dependent T_0 corresponds to multiple scenarios of kinetic freeze-out [15, 16, 28, 29], during both particle formation and kinetic freeze-out processes.

Based on our research experiences [66-70], an examination of the excitation functions for these four parameters reveals a consistent trend. As collision energy increases, these excitation functions rise rapidly within an energy range below approximately 7.7 GeV; beyond this threshold (greater than ~ 7.7 GeV), their increase becomes more gradual. Subsequently, at several tens of GeV (e.g., around 39 GeV), fluctuations occur in these trends or slight changes in growth rates may be observed.

According to properties associated with Quark-Gluon Plasma (QGP) formed in high-energy collisions, QGP can be classified into three types [71]. A QGP in the usual sense is generated in collisions occurring within an energy range from 7.7 to 39 GeV; a weakly coupled QGP (wQGP) forms at energies below 7.7 GeV; whereas a strongly coupled QGP (sQGP) emerges at energies above 39 GeV. There exists a critical endpoint below 7.7 GeV for the formation of wQGP. It is anticipated that larger volumes of sQGP can be generated at higher energies, such as hundreds of GeV and TeV.

5. Summary and conclusions

In summary, this article reviews the inconsistent results regarding thermal parameters derived from various models. To address these discrepancies, we employ model-independent parameters: initial temperature T_i , effective temperature T , kinetic freeze-out temperature T_0 , and average transverse flow velocity β_T . These parameters are determined based on either the average transverse momentum $\langle p_T \rangle$ or the root-mean-square transverse momentum $\sqrt{\langle p_T^2 \rangle}$. Specifically, we propose using: $T_i \approx \sqrt{\langle p_T^2 \rangle}/2$, $T = \langle p_T \rangle$, $T_0 = \langle p_T \rangle/3.07$, and $\beta_T = (2.07/3.07)\langle p_T \rangle/m_0\langle \gamma \rangle$, in data analyses pertaining to high-energy collisions; some of these relationships are drawn from existing literature. This proposal leads to $T_0 =$

$(m_0 \langle \gamma \rangle / 2.07) \beta_T$. By implementing this approach, completely consistent results can be achieved.

To conclude, our analyses indicate that the model-independent parameters in central collisions exceed those observed in peripheral collisions. Additionally, measurements within the central rapidity region surpass those found in the forward/backward rapidity regions. Furthermore, values at high energy (e.g., 200 GeV) are greater than those at low energy (e.g., 10 GeV), and measurements from large collision systems (i.e., nucleus-nucleus collisions) are higher than those from small collision systems (i.e., proton-proton and proton-nucleus collisions). As collision energy increases, excitation functions for all four parameters rise rapidly within a range smaller than approximately 7.7 GeV but increase more slowly beyond this threshold. At higher energies (>39 GeV), fluctuations occur in the trends of these four excitation functions or exhibit slight changes in their growth rates.

In this proposal, while $\langle p_T \rangle$ and $\sqrt{\langle p_T^2 \rangle}$ are independent of any specific model, they demonstrate dependence on particle mass. These dependencies result in T_i exhibiting a mass-dependent multi-scenario for the initial state, whereas T_0 and β_T reveal a mass-dependent multi-scenario for kinetic freeze-out. The formation and emission of various types of particles do not occur simultaneously; generally, the formation and emission of massive particles precede those of lighter particles during the evolution of the collision system. However, instances where these processes interweave, either occurring earlier or later, can also arise. It is challenging to definitively ascertain whether a single- or two-temperature scenario characterizes both the initial state and kinetic freeze-out; nonetheless, it can be concluded that there exists a mass-dependent multi-temperature scenario.

Data Availability

Data sharing not applicable to this article as no data sets were generated during the current study. The data used to support the findings of this study and some outcome or conclusive statements are included within the article and are cited at relevant places within the text as references.

Ethical Approval

The authors declare that they are in compliance with ethical standards regarding the content of this paper.

Disclosure

The funding agencies have no role in the design of the study; in the collection, analysis, or interpretation of the data; in the writing of the manuscript; or in the decision to publish the results.

Conflicts of Interest

The authors declare that there are no conflicts of interest regarding the publication of this paper.

Supplementary Material

There is no supplementary material in this article.

Acknowledgments

The work of Shanxi Group was supported by the National Natural Science Foundation of China under Grant No. 12147215, the Shanxi Provincial Basic Research Program (Natural Science Foundation) under Grant No. 202103021224036, and the Fund for Shanxi “1331 Project” Key Subjects Construction. The work of K.K.O. was supported by the Agency of Innovative Development under the Ministry of Higher Education, Science and Innovations of the Republic of Uzbekistan within the fundamental project No. F3-20200929146 on analysis of open data on heavy-ion collisions at RHIC and LHC.

References

- [1] M. Gyulassy and L. D. McLerran, “New forms of QCD matter discovered at RHIC,” *Nuclear Physics A*, vol. 750, no. 1, pp. 30-63, 2005.
- [2] STAR Collaboration, S. S. Adler et al., “Identified charged particle spectra and yields in Au+Au collisions at $\sqrt{s_{NN}} = 200$ GeV,” *Physical Review C*, vol. 69, no. 3, article 034909, 2004.
- [3] D. D. Chinellato, “Strangeness in Quark Matter 2019: experimental highlights,” *Springer Proceedings in Physics*, vol. 250, pp. 527-533, 2020.
- [4] J. Blair and for the ALICE Collaboration, “Strangeness production with respect to high momentum hadrons in pp and p-Pb collisions with ALICE at the LHC,” *Springer Proceedings in Physics*, vol. 250, pp. 225-229, 2020.
- [5] O. Panova, M. Lewicki, and for the NA61/SHINE collaboration, “System size and energy dependence of proton rapidity spectra from NA61/SHINE at the CERN SPS,” *EPJ Web of Conferences*, vol. 274, p. 05004, 2022.
- [6] I. Vassiliev and for the CBM Collaboration, “Perspectives on strangeness physics with the CBM Experiment at FAIR,” *Springer Proceedings in Physics*, vol. 250, pp. 495-499, 2020.
- [7] V. Kekelidze, V. Kolesnikov, V. Matveev, and A. Sorin, “Status and prospects at NICA,” *Springer Proceedings in Physics*, vol. 250, pp. 503-508, 2020.
- [8] S. R. Nayak, S. Pandey, and B. K. Singh, “Beam energy dependence of transverse momentum distribution and elliptic flow in Au-Au collisions using HYDJET++ model,” 2024, <https://arxiv.org/abs/2405.03174>.
- [9] A. S. Parvan, “Hadron transverse momentum distributions in the Tsallis statistics with escort

- probabilities,” *Journal of Physics G*, vol. 50, no. 12, article 125002, 2023.
- [10] M. Waqas, W. Bietenholz, M. Bouzidi, M. Ajaz, A. A. K. Haj Ismail, and T. Saidani, “Analyzing the correlation between thermal and kinematic parameters in various multiplicity classes within 7 and 13 TeV pp collisions,” *Journal of Physics G*, vol. 51, no. 7, article 075102, 2024.
- [11] S. Chatterjee, S. Das, L. Kumar, D. Mishra, B. Mohanty, R. Sahoo, and N. Sharma, “Freeze-out parameters in heavy-ion collisions at AGS, SPS, RHIC, and LHC energies,” *Advances in High Energy Physics*, vol. 2015, Article ID 349013, 20 pages, 2015.
- [12] T.-T. Duan, P.-P. Yang, P.-C. Zhang, H.-L. Lao, F.-H. Liu, and K. K. Olimov, “Comparing effective temperatures in standard, Tsallis, and q-dual statistics from transverse momentum spectra of identified light charged hadrons produced in gold–gold collisions at RHIC energies,” 2024, <https://arxiv.org/abs/2410.19266>.
- [13] Z. B. Tang, Y. C. Xu, L. J. Ruan, G. van Buren, F. Q. Wang, and Z. B. Xu, “Spectra and radial flow at RHIC with Tsallis statistics in a Blast-Wave description,” *Physical Review C*, vol. 79, no. 5, article 051901(R), 2009.
- [14] S. Chatterjee, B. Mohanty, and R. Singh, “Freezeout hypersurface at energies available at the CERN Large Hadron Collider from particle spectra: flavor and centrality dependence,” *Physical Review C*, vol. 92, no. 2, article 024917, 2015.
- [15] S. Chatterjee and B. Mohanty, “Production of light nuclei in heavy ion collisions within multiple freezeout scenario,” *Physical Review C*, vol. 90, no. 3, article 034908, 2014.
- [16] D. Thakur, S. Tripathy, P. Garg, R. Sahoo, and J. Cleymans, “Indication of a differential freeze-out in proton-proton and heavy-ion collisions at RHIC and LHC energies,” *Advances in High Energy Physics*, vol. 2016, Article ID 4149352, 13 pages, 2016.
- [17] M. Waqas, G.-X. Peng, and F.-H. Liu, “An evidence of triple kinetic freezeout scenario observed in all centrality intervals in Cu-Cu, Au-Au and Pb-Pb collisions at high energies,” *Journal of Physics G*, vol. 48, no. 7, article 075108, 2021.
- [18] E. Schnedermann, J. Sollfrank, and U. Heinz, “Thermal phenomenology of hadrons from 200A GeV S+S collisions,” *Physical Review C*, vol. 48, no. 5, pp. 2462-2475, 1993.
- [19] STAR Collaboration, B. I. Abelev et al., “Systematic measurements of identified particle spectra in pp, d+Au, and Au+Au collisions at the STAR detector,” *Physical Review C*, vol. 79, no. 3, article 034909, 2009.
- [20] STAR Collaboration, B. I. Abelev et al., “Identified particle production, azimuthal anisotropy, and interferometry measurements in Au+Au collisions at $\sqrt{s_{NN}}=9.2$ GeV,” *Physical Review C*, vol. 81, no. 2, article 024911, 2010.
- [21] T. Bhattacharyya, J. Cleymans, A. Khuntia, P. Pareek, and R. Sahoo, “Radial flow in non-extensive thermodynamics and study of particle spectra at LHC in the limit of small (q-1),” *The European Physical Journal A*, vol. 52, p. 30, 2016.
- [22] S. Takeuchi, K. Murase, T. Hirano, P. Huovinen, and Y. Nara, “Effects of hadronic

- rescattering on multistrange hadrons in high-energy nuclear collisions,” *Physical Review C*, vol. 92, no. 4, article 044907, 2015.
- [23] H. Heiselberg and A. M. Levy, “Elliptic flow and Hanbury-Brown-Twiss correlations in noncentral nuclear collisions,” *Physical Review C*, vol. 59, no. 5, pp. 2716-2727, 1999.
- [24] U. W. Heinz, “Concepts of heavy-ion physics,” Lecture Notes for lectures presented at the 2nd CERN-Latin-American School of High-Energy Physics, June 1-14, 2003, San Miguel Regla, Mexico, 2004, <https://arxiv.org/abs/hep-ph/0407360>.
- [25] R. Russo, “Measurement of D^+ meson production in p-Pb collisions with the ALICE detector,” Ph.D. Thesis, Universita degli Studi di Torino, Italy, 2015, <https://arxiv.org/abs/1511.04380>.
- [26] H.-L. Lao, F.-H. Liu, B.-C. Li, and M.-Y. Duan, “Kinetic freeze-out temperatures in central and peripheral collisions: which one is larger?,” *Nuclear Science and Techniques*, vol. 29, no. 6, p. 82, 2018.
- [27] H.-L. Lao, F.-H. Liu, B.-C. Li, M.-Y. Duan, and R. A. Lacey, “Examining the model dependence of the determination of kinetic freeze-out temperature and transverse flow velocity in small collision system,” *Nuclear Science and Techniques*, vol. 29, no. 11, p. 164, 2018.
- [28] H.-L. Lao, H.-R. Wei, F.-H. Liu, and R. A. Lacey, “An evidence of mass-dependent differential kinetic freeze-out scenario observed in Pb-Pb collisions at 2.76 TeV,” *The European Physical Journal A*, vol. 52, no. 7, p. 203, 2016.
- [29] M. Waqas, F.-H. Liu, S. Fakhraddin, and M. A. Rahim, “Possible scenarios for single, double, or multiple kinetic freeze-out in high-energy collisions,” *Indian Journal of Physics*, vol. 93, no. 10, pp. 1329-1343, 2019.
- [30] J. Cleymans and D. Worku, “Relativistic thermodynamics: transverse momentum distributions in high-energy physics,” *The European Physical Journal A*, vol. 48, no. 11, p. 160, 2012.
- [31] PHENIX Collaboration, S. S. Adler et al., “Identified charged particle spectra and yields in Au+Au collisions at $\sqrt{s_{NN}}=200$ GeV,” *Physical Review C*, vol. 69, no. 3, article 034909, 2004.
- [32] P. Koch, J. Rafelski, and W. Greiner, “Strange hadron in hot nuclear matter,” *Physics Letters B*, vol. 123, nos. 3-4, pp. 321-330, 1983.
- [33] P. Braun-Munzinger, D. Magestro, K. Redlich, and J. Stachel, “Hadron production in Au-Au collisions at RHIC,” *Physics Letters B*, vol. 518, nos. 1-2, pp. 41-46, 2001.
- [34] P. Braun-Munzinger, J. Stachel, J. P. Wessels, and N. Xu, “Thermal equilibration and expansion in nucleus-nucleus collisions at the AGS,” *Physics Letters B*, vol. 344, nos. 1-4, pp. 43-48, 1995.
- [35] A. Andronic, P. Braun-Munzinger, and J. Stachel, “Thermal hadron production in relativistic nuclear collisions: the hadron mass spectrum, the horn, and the QCD phase

- transition,” *Physics Letters B*, vol. 673, no. 2, pp. 142-145, 2009.
- [36] J. Cleymans, H. Oeschler, and K. Redlich, “Influence of impact parameter on thermal description of relativistic heavy ion collisions at (1-2)A GeV,” *Physical Review C*, vol. 59, no. 3, pp. 1663-1673, 1999.
- [37] P. Braun-Munzinger, I. Heppe, and J. Stachel, “Chemical equilibration in Pb+Pb collisions at the SPS,” *Physics Letters B*, vol. 465, nos. 1-4, pp. 15-20, 1999.
- [38] J. Manninen and F. Becattini, “Chemical freeze-out in ultra-relativistic heavy ion collisions at $\sqrt{s_{NN}}=130$ and 200 GeV,” *Physical Review C*, vol. 78, no. 5, p. 054901, 2008.
- [39] A. Andronic, P. Braun-Munzinger, and K. Redlich, “Decoding the phase structure of QCD via particle production at high energy,” *Nature*, vol. 561, no. 7723, pp. 321-330, 2018.
- [40] S. Gupta, D. Mallick, D. K. Mishra, B. Mohanty, and N. Xu, “Freeze-out and thermalization in relativistic heavy ion collisions,” 2020, <https://arxiv.org/abs/2004.04681>.
- [41] E. K. G. Sarkisyan and A. S. Sakharov, “Multihadron production features in different reactions,” *AIP Conference Proceedings*, vol. 828, no. 1, pp. 35-41, 2006.
- [42] E. K. G. Sarkisyan and A. S. Sakharov, “Relating multihadron production in hadronic and nuclear collisions,” *The European Physical Journal C*, vol. 70, no. 3, pp. 533-541, 2010.
- [43] A. N. Mishra, R. Sahoo, E. K. G. Sarkisyan, and A. S. Sakharov, “Effective-energy budget in multiparticle production in nuclear collisions,” *The European Physical Journal C*, vol. 74, no. 11, p. 3147, 2014.
- [44] E. K. G. Sarkisyan, A. N. Mishra, R. Sahoo, and A. S. Sakharov, “Multihadron production dynamics exploring the energy balance in hadronic and nuclear collisions,” *Physical Review D*, vol. 93, no. 5, article 054046, 2016.
- [45] E. K. G. Sarkisyan, A. N. Mishra, R. Sahoo, and A. S. Sakharov, “Centrality dependence of midrapidity density from GeV to TeV heavy-ion collisions in the effective-energy universality picture of hadroproduction,” *Physical Review D*, vol. 94, no. 1, article 011501, 2016.
- [46] E. K. Sarkisyan-Grinbaum, A. N. Mishra, R. Sahoo, and A. S. Sakharov, “Effective-energy universality approach describing total multiplicity centrality dependence in heavy-ion collisions,” *EPL (Europhysics Letters)*, vol. 127, no. 6, article 62001, 2019.
- [47] A. N. Mishra, A. Ortiz, and G. Pać, “Intriguing similarities of high- p_T particle production between pp and A-A collisions,” *Physical Review C*, vol. 99, no. 3, article 034911, 2019.
- [48] P. Castorina, A. Iorio, D. Lanteri, H. Satz, and M. Spusta, “Universality in hadronic and nuclear collisions at high energy,” *Physical Review C*, vol. 101, no. 5, article 054902, 2020.
- [49] C. Tsallis, “Possible generalization of Boltzmann-Gibbs statistics,” *Journal of Statistical Physics*, vol. 52, no. 1-2, pp. 479-487, 1988.
- [50] C. Tsallis, “Nonadditive entropy and nonextensive statistical mechanics -- an overview after 20 years,” *Brazilian Journal of Physics*, vol. 39, no. 2, pp. 337-356, 2009.
- [51] T. S. Biró, G. Purcsel, and K. Ürmösy, “Non-extensive approach to quark matter,” *The*

- European Physical Journal A*, vol. 40, no. 3, pp. 325-340, 2009.
- [52] H. Zheng and L. Zhu, “Comparing the Tsallis distribution with and without thermodynamical description in p+p collisions,” *Advances in High Energy Physics*, vol. 2016, Article ID 9632126, 10 pages, 2016.
 - [53] R. Gupta and S. Jena, “Model comparison of the transverse momentum spectra of charged hadrons produced in PbPb collision at $\sqrt{s_{NN}}=5.02$ TeV,” *Advances in High Energy Physics*, vol. 2024, Article ID 5482034, 11 pages, 2024.
 - [54] J. Cleymans and M. W. Paradza, “Tsallis statistics in high energy physics: chemical and thermal freeze-outs,” *Physics*, vol. 2, no. 4, pp. 654-664, 2020.
 - [55] A. S. Parvan, “Equivalence of the phenomenological Tsallis distribution to the transverse momentum distribution of q-dual statistics,” *The European Physical Journal A*, vol. 56, no. 4, p. 106, 2020.
 - [56] F. G. Gardim, G. Giacalone, M. Luzum, and J. Y. Ollitrault, “Thermodynamics of hot strong-interaction matter from ultrarelativistic nuclear collisions,” *Nature Physics*, vol. 16, no. 6, pp. 615-619, 2020.
 - [57] G. Giacalone, “A matter of shape: seeing the deformation of atomic nuclei at high-energy colliders,” Ph.D. Thesis, Université Paris-Saclay, Paris, France, 2021, <https://arxiv.org/abs/2101.00168>.
 - [58] M. Waqas and B.-C. Li, “Kinetic freeze-out temperature and transverse flow velocity in Au-Au collisions at RHIC-BES energies,” *Advances in High Energy Physics*, vol. 2020, Article ID 1787183, 14 pages, 2020.
 - [59] L. J. Gutay, A. S. Hirsch, R. P. Scharenberg, B. K. Srivastava, and C. Pajares, “Deconfinement in small systems: clustering of color sources in high multiplicity pp collisions at $\sqrt{s}=1.8$ TeV,” *International Journal of Modern Physics E*, vol. 24, no. 12, article 1550101, 2015.
 - [60] R. P. Scharenberg, B. K. Srivastava, and C. Pajares, “Exploring the initial stage of high multiplicity proton-proton collisions by determining the initial temperature of the quark-gluon plasma,” *Physical Review D*, vol. 100, no. 11, article 114040, 2019.
 - [61] P. Sahoo, S. De, S. K. Tiwari, and R. Sahoo, “Energy and centrality dependent study of deconfinement phase transition in a color string percolation approach at RHIC energies,” *The European Physical Journal A*, vol. 54, no. 8, p. 136, 2018.
 - [62] M. Waqas and F.-H. Liu, “Centrality dependence of kinetic freeze-out temperature and transverse flow velocity in high energy nuclear collisions,” *Indian Journal of Physics*, vol. 96, no. 4, pp. 1217-1235, 2022.
 - [63] J.-Y. Chen, M.-Y. Duan, F.-H. Liu, and K. K. Olimov, “Multi-source thermal model describing multi-region structure of transverse momentum spectra of identified particles and parameter dynamics of system evolution in relativistic collisions,” *Indian Journal of Physics*, vol. 98, no. 7, pp. 2493-2505, 2024.

- [64] P.-P. Yang, F.-H. Liu, and K. K. Olimov, “Rapidity and energy dependencies of temperatures and volume extracted from identified charged hadron spectra in proton-proton collisions at a Super Proton Synchrotron (SPS),” *Entropy*, vol. 25, no. 12, p. 1571, 2023.
- [65] J.-Y. Chen, M.-Y. Duan, F.-H. Liu, and K. K. Olimov, “Extracting kinetic freeze-out properties in high-energy collisions using a multisource thermal model,” *Advances in High Energy Physics*, vol. 2024, Article ID 9938669, 14 pages, 2024.
- [66] L.-L. Li and F.-H. Liu, “Energy dependent kinetic freeze-out temperature and transverse flow velocity in high energy collisions,” *The European Physical Journal A*, vol. 54, no. 10, p. 169, 2018.
- [67] L.-L. Li and F.-H. Liu, “Kinetic freeze-out properties from transverse momentum spectra of pions in high energy proton-proton collisions,” *Physics*, vol. 2, no. 2, pp. 277-308, 2020.
- [68] M. Waqas, F.-H. Liu, R.-Q. Wang, and I. Siddique, “Energy scan/dependence of kinetic freeze-out scenarios of multi-strange and other identified particles in central nucleus-nucleus collisions,” *The European Physical Journal A*, vol. 56, no. 7, p. 188, 2020.
- [69] L.-L. Li, F.-H. Liu, M. Waqas, R. Al-Yusufi, and A. Mujeer, “Excitation functions of related parameters from transverse momentum (mass) spectra in high-energy collisions,” *Advances in High Energy Physics*, vol. 2020, Article ID 5356705, 21 pages, 2020.
- [70] X.-H. Zhang, Y.-Q. Gao, F.-H. Liu, and K. K. Olimov, “Thermal freeze-out parameters and pseudoentropy from charged hadron spectra in high-energy collisions,” *Advances in High Energy Physics*, vol. 2022, Article ID 7499093, 36 pages, 2022.
- [71] K. A. Mamo, “Net-proton number cumulants in strongly and weakly coupled QGP,” 2024, <https://arxiv.org/abs/2407.06327>.